Spectroscopic and relaxation character of the $^3P_0$-$^3H_4$ transition in LaF$_3$:Pr^{3+} measured by photon echoes

Y. C. Chen, K. Chiang, and S. R. Hartmann

Columbia Radiation Laboratory, Department of Physics, Columbia University, New York, New York 10027

(Received 16 July 1979)

The hyperfine structure and relaxation character of the terminal levels of the $^3P_0$-$^3H_4$ (4777 Å) transition in LaF$_3$:Pr^{3+} (0.03 at. %) were studied using the photon-echo technique. Using two independent nitrogen-laser pumped dye lasers we have observed modulated photon echoes for pulse separations over a $\sim$10-μsec range. In this interval our modulated photon echoes decay in a simple exponential manner by a factor of 10^5 and yield a homogeneous linewidth of 70 kHz [full width at half maximum (FWHM)]. Fourier transformation of the echo-modulation data yields directly the nuclear level splittings and their associated linewidths in the $^3P_0$ and $^3H_4$ states. In the $^3P_0$ ($^3H_4$) state the nuclear splittings are 0.73 and 1.12 MHz (8.48 and 16.68 MHz). The measurements for the nuclear level splittings and associated linewidths in the $^3H_4$ state are in excellent agreement with those obtained from the optical-rf double-resonance experiments of Erickson. We find that the calculated echo modulation is a sensitive function of the relative orientation of the principal axes associated with the ground- and excited-state Hamiltonians. By comparing our experimental and calculated echo-modulation patterns we are able to determine their relative orientations.

I. INTRODUCTION

The Pr^{3+} ion in crystals of LaF$_3$ substitutes for the La atom and exhibits an absorption and emission spectrum characteristic of an ion whose energy levels are nondegenerate.[1] Although the crystal structure of LaF$_3$ is somewhat controversial, the most likely model appears to be that proposed by Mansmann[2] and Zalkin et al.[3] They suggest $P3c1$-D_{3d}^3 which has a trigonal structure with six molecules per unit cell and which exhibits C_2 point symmetry about each of the three inequivalent La sites. The twofold axis of C_2 is normal to the crystal c axis. Since the Pr^{3+} ion has two unpaired $4f$ electrons, the low symmetry at the La site removes all the degeneracy of the energy eigenstates and requires that for each eigenstate $\langle \vec{J} \rangle = 0$ where $\vec{J}$ is the electronic angular momentum operator. To first order then, the Pr^{3+} ions have no electronic magnetism and one might expect that they would be well isolated. It follows that in any coherent optical transient experiment they should behave in a simple manner. It is not surprising then that Takeuchi and Szabo[4] found that, in contrast to the case of ruby,[5] it is possible to observe photon echoes in LaF$_3$:Pr^{3+} without the application of an external magnetic field. They also found, in accord with expectations, that with the 38-nsec excitation pulse separation time τ they used, an applied magnetic field in the range $0 < H < 500$ G had no effect on the photon-echo intensity. Further investigations by Takeuchi showed the echo to decay in a simple exponential manner as $\exp(-\tau/\tau_0)$ for 60

nsec $< \tau < 220$ nsec, with $\tau_0 = 100$ nsec.[6] The small value of τ_0 was anomalous in view of the isolated nature of the Pr^{3+} ion. These experiments were performed on the $^3H_4$-$^3P_0$ (4777 Å) transition at liquid-helium temperatures.

Magnetic field effects on photon-echo intensity were first observed in LaF$_3$:Pr^{3+} by Chen and Hartmann[7] who worked at larger values of τ and H. They made an estimate of the second-order hyperfine interaction based on published susceptibility measurements in PrF$_3$,[8] which allowed them to account for the order of magnitude of the effects they observed, and also explain the null result of Takeuchi and Szabo. The optical-rf double-resonance experiment of Erickson[9] provided a direct measurement of the level splittings of the ground $^3H_4$ state, and gave an accurate representation of the ground-state Hamiltonian

$$\mathcal{H}_g = P_g \left[I_z^2 + \frac{\eta_g}{3}(I_x^2 - I_y^2) \right] , \qquad (1)$$

with $P_g = 4.185$ MHz and $\eta_g = 0.105$. Subsequent double-resonance experiments of Erickson confirmed this result and also provided the splitting of the $^1D_2$ excited state.[10] No experiments were performed to resolve splittings in the $^3P_0$ state.

The first observation of a nonexponential decay for the echo intensity versus τ in LaF$_3$:Pr^{3+} was reported by Chen et al.[11] who found a sharp rephasing at $\tau \cong 240$ nsec, just beyond the region studied by Takeuchi.[2] They also reported the observation of echoes in the $^1D_2$-$^3H_4$ transition (5925 Å) which were

modulated at the inverse of 8.47 MHz, the $^3H_4$ ground-state splitting frequency. More recent experiments by Chen et al.[12] and Morsink and Wiersma[13] using independently triggered nitrogen-pumped dye lasers have confirmed the observed rephasing at 240 nsec and have shown that the echo-decay envelope is more complex than had previously been expected. The Columbia group has been able to make an accurate determination of the $^3P_0$ excited-state Hamiltonian.[12] They found

$$\mathcal{K}_e = P_e[I_Z^2 + \tfrac{1}{3}\eta_e(I_X^2 - I_Y^2)] \ , \qquad (2)$$

with P_e and η_e given as 0.312 MHz and 0.5, respectively, very close to the values of $P_e = 0.293$ MHz and $\eta_e = 0.516$ determined in this paper. The use of lower case and upper case subscripted operators in Eqs. (1) and (2) reflects the fact that the principal axes of the Hamiltonian $\mathcal{K}_g$ and $\mathcal{K}_e$ are not identical.[11] The echo rephasing observed early on at $\tau = 240$ nsec was an indication that the homogeneous linewidth is quite narrow. Indeed, the echo envelopes observed for the $^3P_0$-$^3H_4$ transition with a 0.01-at.% crystal implies a homogeneous linewidth of only 40 kHz.[12] On the other hand, for a 1.0-at.% crystal the inferred linewidth was 240 kHz.[12] Recent free-induction decay experiments by DeVoe et al.[14] using a very stable laser have been performed on the $^3H_4$-$^1D_2$ transition, and have shown that for that transition, the homogeneous linewidth can be as narrow as 20 kHz in an external magnetic field of 76 G.

Finally it should be noted that the character of the 200-kHz linewidth of the nuclear hyperfine transitions has also been clarified by recent echo experiments[11] as well as by experiments by Shelby et al.[15] which have optically detected coherent transients in the nuclear hyperfine levels. Both these experiments have shown the 200-kHz nuclear linewidth to be inhomogeneous.

The above discussion shows that the photon-echo technique is capable of generating a large amount of information without imposing great demands on the experimental apparatus. All the experiments of the Columbia group were performed with lasers whose linewidths were of the order of 10 GHz and whose 7-nsec-long excitation pulses were therefore multimode. Yamagishi and Szabo[16] have studied photon-echo behavior in the $^3H_4$-$^3P_0$ transition with a narrow 250-MHz linewidth laser. The only advantage, albeit an important one, of the narrow linewidth is that it enables one to generate and study echoes in different parts of the inhomogeneous Pr^{3+} line separately. They report no dependence of the relaxation behavior as a function of laser frequency.

An important feature of the photon-echo technique is that the echo signals are very large. It can be

shown, for example, that the number of photons N in the echo is related to the number of photons N_{ex} required to equalize the ground- and excited- state population by the formula $N = (\alpha L/\pi)N_{ex}$ where α is the absorption coefficient and L is the sample length.[17] This formula is only strictly valid for $\alpha L \ll 1$ but it shows that in principle the echo intensity need only be a few orders of magnitude less intense than the excitation pulses necessary to generate them. In the experiments reported herein we are able to observe echoes over an intensity range of 10^5:1 thereby allowing the measurement of fine structural detail and narrow linewidths.

The major problem of working with a technique whose data contains a wide variety of information is associated with the information extraction process. Echo modulation in ruby is quite complex[18] but the photon-echo—nuclear double-resonance (PENDOR) technique[19] allows a direct means of separately obtaining the interaction parameters of the Cr^{3+} ion with each of some 24 nearest neighbors. In the case of $LaF_3:Pr^{3+}$ we have Fourier-transformed echo-modulation data and have found that we can thereby obtain directly the Hamiltonians $\mathcal{K}_e$ and $\mathcal{K}_g$ as well as the linewidths of the nuclear hyperfine transitions in the ground and excited states. From the overall observed exponential decay of the echo-modulation pattern we obtain a 70-kHz homogeneous linewidth for our 0.03-at.% sample. The only remaining unknown factors are the relative sign of P_e and P_g and the relative orientation of the principal axes for $\mathcal{K}_e$ and $\mathcal{K}_g$. As will be shown, we are able to determine the relative orientation of the principal axes by calculating the effect of the orientation on the echo-modulation pattern and comparing our calculated pattern with the experimentally observed one.

II. EXPERIMENTAL APPARATUS

The schematic diagram of the apparatus used for our photon-echo-modulation experiment is shown in Fig. 1. The two laser excitation pulses are provided by two independent nitrogen-laser pumped dye lasers, triggered by EG&G HY-1102 grounded-grid thyratrons. The time jitter of the lasers is reduced to less than 2 nsec by appropriately adjusting the grid bias voltages and by applying to the cathodes of the thyratrons 1-kV pulses whose rise times are less than 10 nsec. One of the dye lasers is of the Hänsch design, the other of a design based on the work of Littman and Metcalf.[20] Both dye lasers produce several hundred watt pulses (at the sample) 10 GHz wide and roughly 7 nsec in duration. Laser excitation pulse separation is adjusted electronically, making it amenable to computer control, and allowing continuous variation and arbitrarily long delay. The laser pulses are combined and focused into the sample. An Ortec
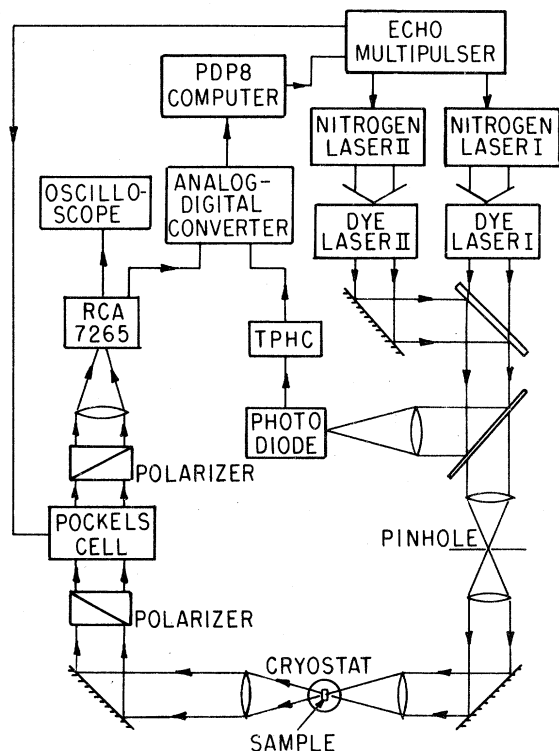
FIG. 1. Schematic diagram of the photon-echo experiment.

FIG. 2. Comparison of the experimental and theoretical photon-echo-modulation pattern. The data was taken for the $^3H_4$-$^3P_0$ transition of a 0.03-at. % crystal of $LaF_3:Pr^{3+}$. The theoretical calculation was made using Eqs. (1) and (2) as the excited- and ground-state Hamiltonians with $P_3 > 0$, $P_g > 0$, $2\Omega^{(g)}/2\pi = 200$ kHz, $2\Omega^{(e)}/2\pi = 20$ kHz, $\hat{X} \parallel \hat{y}$ and $\theta_{\hat{z}\hat{z}} = 35°$. An exponential damping factor $\exp(-\tau/1.2 \ \mu sec)$ has also been included.

model 457 biased time-to-pulse-height converter, which has been carefully calibrated with respect to a frequency synthesizer (HP model 5100A) to an accuracy of 0.1%, is used to measure the excitation pulse separation. The excitation pulses are prevented from saturating the RCA-7265 photomultiplier detector by using two stages of crossed polarizers and Pockel cells. Echo signals are stored and averaged by a PDP8/E computer. The crystal is mounted in a variable temperature cryostat, and all measurements are made at temperatures below 3 °K where spin-lattice relaxation effects are negligible. The major improvement in this apparatus over that described previously is in the replacement of the Kerr cell shutters by Pockel cell shutters.[12]

III. RESULTS AND ANALYSIS

In Fig. 2 we present two traces. The upper trace is an experimental observation of echo intensity versus pulse separation for the $^3H_4$-$^3P_0$ transition of the Pr^{3+} ion (0.03 at. %) in LaF_3. The lower trace is a theoretical result which will be discussed later. The echo-modulation pattern is characterized by a high-frequency component which damps out with a time constant of the order of 2.0 μsec and a much longer-lived low-frequency component. There is also an
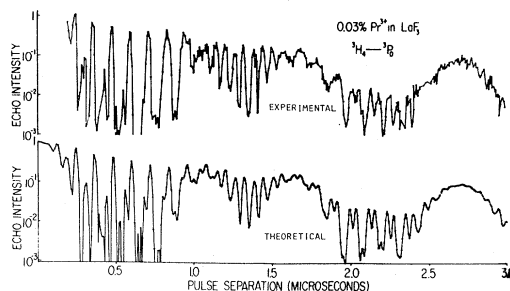
overall exponential decay component with a time constant of 1.2 μsec. This latter feature is more apparent in Fig. 3, where the traces of Fig. 2 are extended to $\tau \cong 10$ μsecs. This figure also displays more of the character of the low-frequency modulations. The data points of Fig. 3 were not connected with a smooth curve as the high-frequency oscillations, on the scale of this figure, merge into a blurry image.

The data shown in Figs. 2 and 3 is consistent with the data we have presented previously.[5] Improvements in experimental technique enable us to observe finer modulation details and to study echo-modulation behavior for greater values of τ. The only noticeably different characteristic of our new
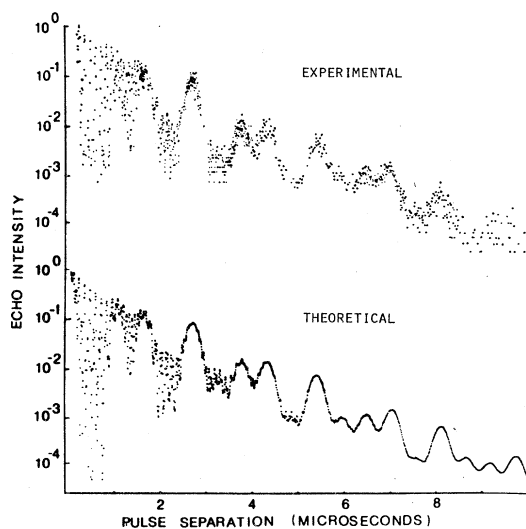

FIG. 3. Comparison of the experimental and theoretical photon-echo-modulation pattern with the traces of Fig. 2 being extended to $\tau = 10$ μsec.

data is the overall rate at which the echo intensity decays. Our previous measurement of this decay time constant gave 40 and 200 kHz for the homogeneous linewidth with the 0.01% and 1.0% samples, respectively. The present observation of a 1.2-μsec time constant in the 0.03% sample corresponds to a linewidth of 70 kHz.

The theory of modulated photon echoes has been discussed by several authors.[21-23] Echo modulation arises from an interference among atomic transitions in a coherently excited multilevel system. Modulation occurs whenever an atomic system is coherently excited into a superposition of nearly degenerate en-

ergy states. For Pr^{3+} in LaF_3 the optical transitions take place between states with no electronic degeneracy and which are only moderately split (in comparison with the bandwidth of the laser excitation pulses) by nuclear hyperfine and electric quadrupole interactions. For such a system the formulation of Grischkowsky and Hartmann[21] is particularly convenient and we use it to analyze echo-modulation behavior.

For atoms with a nuclear-spin Hamiltonian $\mathcal{H}_g$ ($\mathcal{H}_e$) associated with the ground (excited) state, the echo is manifest in a rephased dipole moment which develops according to

$$\vec{P}(2\tau) = \vec{P}(0)(2I+1)^{-1}\text{Tr}[\exp(-i\tau\mathcal{H}_g/\hbar)\exp(-i\tau\mathcal{H}_e/\hbar)\exp(i\tau\mathcal{H}_g/\hbar)\exp(i\tau\mathcal{H}_e/\hbar)] \quad , \tag{3}$$

where I is the spin of the atomic nucleus. If we define $W = U_e U_g^{-1}$, where $U_e\mathcal{H}_e U_e^{-1} = \mathcal{H}_{De}$, $U_g\mathcal{H}_g U_g^{-1} = \mathcal{H}_{Dg}$ and $\mathcal{H}_{Dg}$, $\mathcal{H}_{De}$ are diagonal, then $\vec{P}(2\tau)$ can be rewritten as

$$\vec{P}(2\tau) = \vec{P}(0)(2I+1)^{-1}\sum_{\alpha,\beta,\gamma,\epsilon=1}^{2I+1}(W)_{\alpha\beta}(W^{-1})_{\beta\gamma}(W)_{\gamma\epsilon}(W^{-1})_{\epsilon\alpha}\cos[(\omega_{\alpha\gamma}^{(e)} - \omega_{\beta\epsilon}^{(g)})\tau]$$

$$= \sum_{\alpha,\beta,\gamma,\epsilon}^{2I+1}\vec{P}_{\alpha\beta\gamma\epsilon}(2\tau) \quad , \tag{4}$$

where $\omega_{\alpha\gamma}^{(e)} = (\mathcal{H}_{De})_{\alpha\alpha} - (\mathcal{H}_{De})_{\gamma\gamma}$ and $\omega_{\beta\epsilon}^{(g)} = (\mathcal{H}_{Dg})_{\gamma\gamma} - (\mathcal{H}_{Dg})_{\epsilon\epsilon}$. In this expression $\vec{P}(2\tau)$ appears as the sum of a series of terms which oscillate at the sum and difference of the frequencies corresponding to the nuclear hyperfine splittings of the ground and excited states. If we assume the various frequencies $\omega_{\alpha\gamma}^{(e)}$ ($\omega_{\beta\epsilon}^{(g)}$) are distributed according to the distribution function $G_{\alpha\gamma}^{(e)}$ ($G_{\beta\tau}^{(g)}$) the net dipole moment which we designate as $\langle\vec{P}(2\tau)\rangle$ is given by

$$\langle\vec{P}(2\tau)\rangle = \int\sum_{\alpha,\beta,\gamma,\epsilon=1}^{2I+1}d\omega_{\alpha\gamma}^{(e)}d\omega_{\beta\epsilon}^{(g)}G_{\alpha\gamma}^{(e)}G_{\beta\epsilon}^{(g)}\vec{P}_{\alpha\beta\gamma\epsilon}(2\tau) \quad . \tag{5}$$

For Lorentzian distribution functions with halfwidths at half maximum of $\Omega_{\alpha\gamma}^{(e)}$ ($\Omega_{\beta\epsilon}^{(g)}$) this reduces to

$$\langle\vec{P}(2\tau)\rangle = \vec{P}(0)(2I+1)^{-1}\sum_{\alpha,\beta,\gamma,\epsilon=1}^{2I+1}(W)_{\alpha\beta}(W^{-1})_{\beta\gamma}(W)_{\gamma\epsilon}(W^{-1})_{\epsilon\alpha}\exp[-(\Omega_{\alpha\gamma}^{(e)} + \Omega_{\beta\epsilon}^{(g)})\tau]\cos(\omega_{\alpha\gamma}^{(e)} - \omega_{\beta\epsilon}^{(g)})\tau \quad . \tag{6}$$

For Pr^{3+} in LaF_3, $I = \frac{5}{2}$ and there are 25 different frequencies $\omega_{\alpha\gamma}^{(e)} - \omega_{\beta\epsilon}^{(g)}$ distributed over the 1296 arrangements of the indices α, β, γ, and ϵ. The echo intensity varies as $\langle\vec{P}(2\tau)\rangle^2$ and it is certainly reasonable to expect that one can obtain a set of W's, ω's, and Ω's with which to fit the data of Figs. 2 and 3. However, since there are so many parameters involved, it is preferable to use a method whereby the parameters are obtained directly. Taking the Fourier transform of $P(2\tau)^2$, i.e.,

$$F[\langle\vec{P}(2\tau)\rangle^2] = \int_0^\infty\langle\vec{P}(2\tau)\rangle^2\cos\omega\tau\,d\tau \tag{7}$$

achieves, in principle, the desired result. One might expect, however, that the complexity of $\langle\vec{P}(2\tau)\rangle$ would frustrate the method. Fortunately the expression for $\vec{P}(2\tau)$ in the case of $LaF_3:Pr^{3+}$ is dominated by the zero frequency term and the single frequency terms. Of these two the zero frequency term is by

far the larger. This situation arises both from the interferences among the matrix elements of W and from the variation in the number of contributions (permutations of the indices α, β, γ, ϵ) to each separate frequency term. There are in fact 144 contributions to the zero frequency term, 96 contributions to each of the single frequency terms, and only 32 contributions to each of the 18 multiple frequency terms having neither $\omega^{(e)}$ or $\omega^{(g)}$ equal to zero. It appears that in analyzing the effect of taking the Fourier transform of the echo intensity we can neglect multiple frequency terms and express Eq. (4) or $\vec{P}(2\tau)$ simply as

$$\vec{P}(2\tau) \simeq \vec{P}(0)\left[A + \sum_{\alpha\neq\gamma}B_{\alpha\gamma}^{(e)}\cos\omega_{\alpha\gamma}^{(e)}\tau + \sum_{\beta\neq\epsilon}B_{\beta\epsilon}^{(g)}\cos\omega_{\beta\epsilon}^{(g)}\tau\right] \quad , \tag{8}$$

with the condition that $A \gg B$.

The Fourier transform of $\langle \overline{P}(2\tau) \rangle^2$ in the region of the single frequency resonances is then given by

$$F[\langle \overline{P}(2\tau) \rangle^2] \approx \sum_{\alpha,\beta,\gamma,\epsilon} (W)_{\alpha\beta}(W^{-1})_{\beta\gamma}(W)_{\gamma\beta}(W^{-1})_{\beta\alpha}G_{\alpha\gamma}^{(e)} + \sum_{\alpha,\beta,\gamma,\epsilon} (W)_{\alpha\beta}(W^{-1})_{\beta\alpha}(W)_{\alpha\epsilon}(W^{-1})_{\epsilon\alpha}G_{\beta\epsilon}^{(g)} . \quad (9)$$

To the extent that this expression is correct, the Fourier transform clearly provides the frequency splittings of the terminal levels as well as the nuclear hyperfine transition linewidths. In Fig. 4 we show the Fourier transform of $\langle \overline{P}(2\tau) \rangle^2 \exp(\tau/1.2 \ \mu sec)$ as a function of the frequency $\nu = \omega/2\pi$. The exponential decay factor is included to weight the data of Fig. 3 uniformly throughout the whole time interval. In obtaining $F[P(2\tau)^2 \exp(\tau/1.2 \ \mu sec)]$ the time integration has been performed from 100 nsec to 3 μsec for frequencies between 8 and 28 MHz, and from 1 to 8 μsec for frequencies below 2 MHz. As shown in Fig. 4, the transform data are dominated by two pairs of three strong lines each satisfying the relation $\omega_1 + \omega_2 = \omega_3$ which is characteristic for $I = \frac{5}{2}$ of a Hamiltonian in quadratic form. The simplicity of this result supports our suggestion that Eq. (9) correctly describes the major resonances. Table I summarizes our results. Note that the resonances at 8.48 and 16.68 MHz sum to the observed resonance at ≈ 25.14 MHz, whereas the resonances at 0.73 and 1.12 MHz sum to the observed resonance at 1.85 MHz. Our observation of the 8.48- and 16.68-MHz resonances confirm the optical-rf double-resonance experiment measurement of the level splittings of the $^3H_4$ ground state as made by Erickson.[9] The 0.73- and 1.12-MHz resonances are new and correspond to the energy splittings of the excited $^3P_0$ state.

From the linewdiths of the Fourier transform peaks we obtain the corresponding linewidths for the nuclear hyperfine transitions. The contribution of the linewidth from the finiteness of the time interval over which the data has been taken must be deducted. The measured widths and their corresponding nuclear transition linewidths have been tabulated in Table I. Our measurement of the full width at half maximum of 220 and 200 kHz for the 8.48- and 16.68-MHz lines is in close agreement with Erickson[9] and Shelby et al.[15] For the excited state we find $2\Omega^{(e)}/2\pi \approx 20$ kHz, in agreement with our previous estimate.[12]

For a complete understanding of the data of Figs. 2 and 3 we require the W matrices or their equivalent, the Hamiltonian $\mathcal{H}_e$ and $\mathcal{H}_g$. Both $\mathcal{H}_e$ and $\mathcal{H}_g$ can be put in a form quadratic in nuclear angular momentum operators and written as shown in Eqs. (1) and (2). From the energy-level splittings we infer that $P_e = \pm 0.293$ MHz and $\eta_e = 0.516$, with $P_g = \pm 4.185$ MHz and $\eta_g = 0.105$. The principal axes $\hat{x}$, $\hat{y}$, $\hat{z}$ and $\hat{X}$, $\hat{Y}$, $\hat{Z}$ have been defined with the largest component of each Hamiltonian along the $\hat{z}$ ($\hat{Z}$) axis. Our use of upper and lower subscripted spin operators reflects our ignorance of the relative orientation of the principal axes for $\mathcal{H}_g$ and $\mathcal{H}_e$. This relative orientation can be determined by its effect on the calculated photon-echo-modulation pattern. We first note that the C_2 symmetry of the La site requires that each Hamiltonian have one principal axis in common. Since the Hamiltonians are quadratic, a rotation of π (or 2π) about the $\hat{C}_2$ axis of one princi-
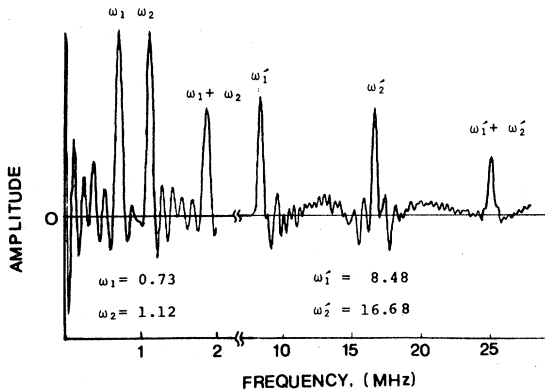

FIG. 4. Fourier spectrum of the echo-modulation data in Fig. 3. The Fourier transform was obtained by performing the time integration from 200 nsec to 3 μsec for frequencies between 8 and 25 MHz, and from 1 to 8 μsec for frequencies below 2 MHz.

TABLE I. Frequency and linewidth measurements of nuclear transitions in the ground $^3H_4$ state and the excited $^3P_0$ states of $LaF_3:Pr^{3+}$.

	Frequency (MHz)	$2\Omega'/2\pi$ (kHz)[a]	$2\Omega/2\pi$ (kHz)[b]
$\omega_1^{(g)}/2\pi$	8.48 ± 0.05	320 ± 20	220 ± 30
$\omega_2^{(g)}/2\pi$	16.68 ± 0.05	310 ± 20	200 ± 30
$\omega_3^{(g)}/2\pi$	25.14 ± 0.05	330 ± 30	240 ± 40
$\omega_1^{(e)}/2\pi$	0.73 ± 0.02	90 ± 5	15 ± 10
$\omega_2^{(e)}/2\pi$	1.12 ± 0.02	90 ± 5	15 ± 10
$\omega_3^{(e)}/2\pi$	1.83 ± 0.02	95 ± 5	25 ± 10

[a]Full width at half maximum measured from Fig. 4.
[b]Nuclear transition linewidth with the contribution from the finiteness of the time interval, T, being deduced. It was obtained by varying Ω so that the width of the central peak of $F(\omega) = \int_0^T e^{-\Omega T} \cos \omega t \ dt$ is equal to $2\Omega'$.

pal axis system, keeping the other fixed, does not change the calculated echo amplitude. There are only $3! = 6$ inequivalent ways in which the two principal axes of both systems are parallel. For each parallel configuration there are three possible orientations of the $\hat{C}_2$ axis. It is easy to show that any rotation about $\hat{C}_2$ away from such a parallel configuration by θ is equivalent to a rotation by $-\theta$. Consider the case where $\hat{z} \parallel \hat{Z} \parallel \hat{C}_2$, and rewrite $\mathcal{K}_g$ in the general form

$$\mathcal{K}_g(\theta) = \exp(-i\theta I_z) P_g [I_z^2 + \tfrac{1}{3}\eta_g/(I_x^2 - I_y^2)] \exp(i\theta I_z)$$

$$= \exp(-i\theta I_z)\mathcal{K}_g(0)\exp(i\theta I_z) \qquad (10)$$

so that

$$\bar{P}(2\tau,\theta) = \bar{P}(0)(2I+1)^{-1}$$

$$\times \mathrm{Tr}\{\exp[-i\tau\mathcal{K}_e(0)/\hbar]\exp[-i\tau\mathcal{K}_g(\theta)/\hbar]$$

$$\times\exp[i\tau\mathcal{K}_e(0)/\hbar]\exp[i\tau\mathcal{K}_g(\theta)/\hbar]\} \quad .(11)$$

But

$$\exp[-i\tau\mathcal{K}_g(\theta)/\hbar] = \exp(-i\theta I_z)\exp[-i\tau\mathcal{K}_g(0)/\hbar]$$

$$\times\exp(i\theta I_z) \quad . \qquad (12)$$

It therefore follows that $\bar{P}(2\tau,\theta) = \bar{P}(2\tau,-\theta)$ since any rotation by π about the x axis leaves both $\mathcal{K}_e(0)$

and $\mathcal{K}_g(0)$ unchanged, but changes $\exp(\pm i\theta I_z)$ to $\exp(\mp i\theta I_z)$. It is therefore possible to construct a map describing all possible axis configurations with each configuration giving rise to a distinctive echo-modulation pattern. This map has six vertices, each corresponding to the principal axes of both systems being parallel. All the vertices are joined by paths along which each system has a principal axis in common and the other axes are successively rotated. In Figs. 5 and 6 we show partial maps obtained in the case of Fig. 5 when P_e and P_g have the same relative sign. For P_e and P_g of opposite sign we obtain Fig. 6. We call these maps partial because, due to lack of space, we only show one point (the midpoint) along the path between any two vertices. In laying this map out in a rectangular form we have not connected the vertices at the top of the page with paths terminating at the bottom of the page. It is to be understood that the path at the bottom right (left) connects with the vertex at the top left (right). This asymmetry is a result of the fact that there is no way to construct this particular kind of map without having two paths cross. In calculating the echo-modulation patterns in Figs. 5 and 6 we have set $\Omega^g = 0$ and $\Omega^e = 0$, i.e., we have neglected damping. The patterns displayed in Figs. 5 and 6 show a widely varying character indicating that it is certainly possi-
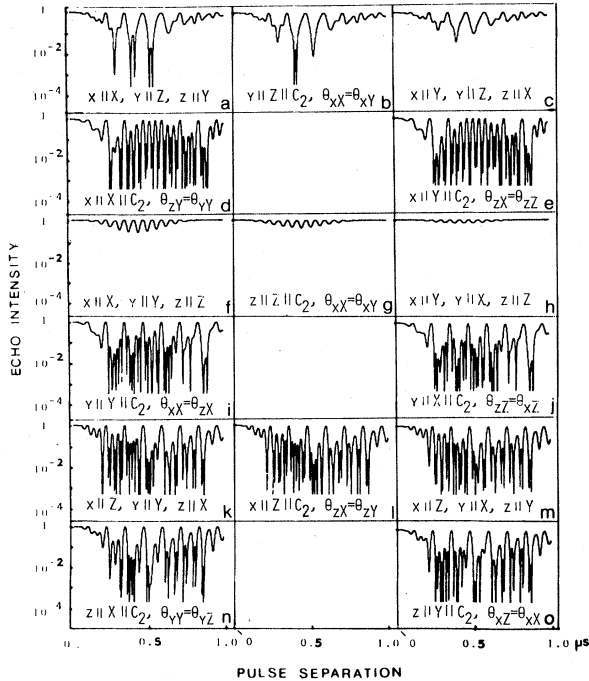

FIG. 5. Map showing the photon-echo-modulation patterns at various possible axis configurations of the excited- and ground-state Hamiltonians (see text). The calculations were made using Eqs. (1) and (2) as the Hamiltonians, with $P_e > 0$, $P_g > 0$, $2\Omega^{(g)}/2\pi = 2\Omega^{(e)}/2\pi = 0$.
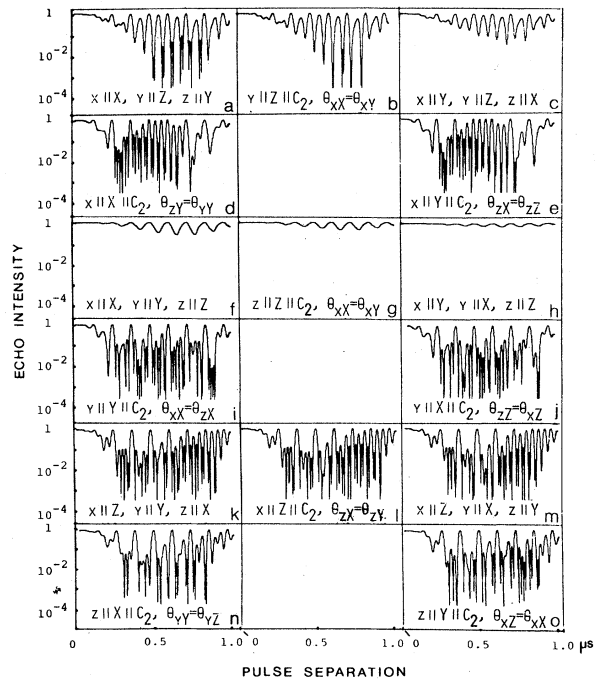

FIG. 6. Map showing the photon-echo-modulation patterns at various possible axis configurations of the excited- and ground-state Hamiltonians. The parameters used are the same as those for Fig. 5 except that $P_g > 0$ and $P_e < 0$.

ble to eliminate by comparison with experimental data many possible principal axes orientations. The symmetric nature of $\mathcal{3C}_g$ which is a consequence of $\eta_g \ll 1$, on the other hand, minimizes the change in the character of the modulation when either $\hat{X}$ or $\hat{Y}$ are interchanged or a rotation is made about the $\hat{Z}$ axis. We find close agreement with experimental data whenever both $\hat{z}$ and $\hat{Z}$ are perpendicular to $\hat{C}_2$ with $\hat{X}$ (or $\hat{Y}$) $\parallel \hat{C}_2 \parallel \hat{y}$ and $20° < \cos^{-1}(|\hat{z} \cdot \hat{Z}|)$ $< 35°$. In this particular region the relative signs of P_e and P_g have little influence on the closeness of the modulation pattern fits. As mentioned above, because of limitations of space we have displayed, in Figs. 5 and 6, only a partial map of modulation patterns for various relative orientations of the ground- and excited-state axes. If we could have presented a more detailed map with patterns for which the relative orientations differ by, for example 5°, rather than 45°, as is the case, then the calculated patterns for the orientations which agree well with the experimental data would lie between those labeled f and i, or between h and j, in Figs. 5 and 6.

In the bottom traces of Figs. 2 and 3 we plot the echo intensity as calculated from $P_e = 0.293$ MHz, $\eta_e = 0.516$, $2\Omega^{(e)}/2\pi = 20$ kHz, $P_g = 4.185$ MHz, $\eta_g = 0.105$, $2\Omega^{(g)}/2\pi = 200$ kHz, $\theta_{\hat{z}\hat{x}} = 35°$ with $\hat{X} \parallel \hat{Y}$, and including the factor $\exp(-\tau/1.2 \ \mu\text{sec})$. The agreement between the theory and the experiment is quite satisfactory. Echo intensity calculated as above but with $\hat{Y} \parallel \hat{y}$ does not differ enough to enable us to favor one over the other. The same is true if we let P_e and P_g have opposite signs.

The presence of the inhomogeneous damping terms $\exp[-(\Omega^{(e)}_{\alpha\gamma} + \Omega^{(g)}_{\beta\epsilon})\tau]$ in Eq. (6) considerably modify the form of the echo intensity modulation envelope. In Fig. 7 we have illustrated this by showing three traces of $\langle P(2\tau)\rangle^2$ using $P_e = 0.293$ MHz, $\eta_e = 0.516$, $P_g = 4.185$ MHz, $\eta_g = 0.105$, and $\theta_{\hat{z}\hat{x}} = 35°$. For the top trace we take $\Omega^{(e)}_{\alpha\gamma}/2\pi$ $= \Omega^{(g)}_{\beta\epsilon}/2\pi = 0$, for the middle trace $2\Omega^{(e)}_{\alpha\gamma}/2\pi = 20$ kHz, $2\Omega^{(g)}_{\beta\epsilon}/2\pi = 200$ kHz, and for the bottom trace, $2\Omega^{(e)}_{\alpha\gamma}/2\pi = 2\Omega^{(g)}_{\beta\epsilon}/2\pi = 200$ kHz. Our analysis shows clearly that $\Omega^{(g)} \gg \Omega^{(e)}$. This result follows from the excited state $^3P_0$ being an electronic singlet susceptible to being split only by nuclear interactions. On the other hand, as discussed previously,[7,11,12] the closeness of the crystal-field-split levels in the $^3H_4$ multiplet gives rise to a sizeable second-order hyperfine interaction[24] and enhanced nuclear magnetism,[24,25] both of which may contribute to line broadening in nuclear transitions. The second-order hyperfine interaction is able to transfer inhomogeneous broadenings associated with the crystal-field-split levels to nuclear levels, since the interaction parameter P_g is inversely proportional to the energy-level separations of the crystal-field levels.[11] The enhanced nuclear magnetism increases the magnetic
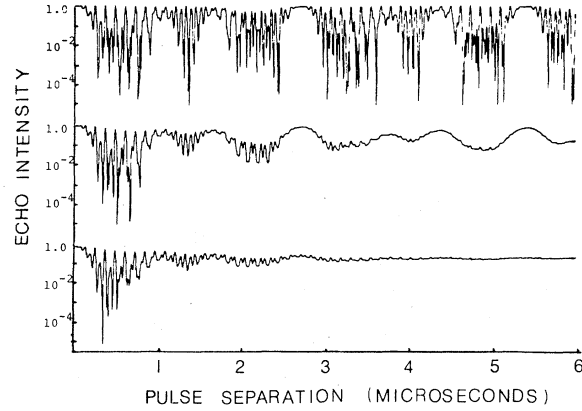

FIG. 7. Comparison of the photon-echo-modulation pattern for different inhomogeneous linewidths for nuclear transitions in the ground and excited states. We use $P_e = 0.293$ MHz, $\eta_e = 0.516$, $P_g = 4.185$ MHz, $\eta_g = 0.105$ and $\theta_{\hat{z}\hat{z}} = 35°$. For the topmost trace we have taken $2\Omega^{(e)}/2\pi = 2\Omega^{(g)}/2\pi = 0$; for the middle trace $2\Omega^{(e)}/2\pi = 2\theta$ kHz, $2\Omega^{(g)}/2\pi = 200$ kHz, and for the bottom trace $2\Omega^{(e)}/2\pi = 2\Omega^{(g)}/2\pi = 200$ kHz.

broadening due to the Pr-F dipolar interaction, because of an additional contribution to the gyromagnetic ratio by the amount of $\gamma_N K_i$ where γ_N is the normal gyromagnetic ratio ($=1.31$ MHz/kG) and K_i is the ith component of the enhancement factor.[25] Theoretical considerations show that the z component of the enhancement factor must lie between 4.5 and 11.5.[12] Since the nuclear wave functions in the $^3H_4$ state are approximately $|\pm\frac{1}{2}\rangle$, $|\pm\frac{3}{2}\rangle$, and $|\pm\frac{5}{2}\rangle$, the linewidths for the 8.47-, 16.7-, and 25.2-MHz lines will have the ratio of 1:1:2 if the magnetic dipolar broadening is dominant, and will have the ratio of 1:2:3 if the second-order hyperfine broadening is dominant. However, our measurement is substantially different from these ratios. The reason for the discrepancy is not understood.

The nuclear quadrupole splittings of the $^3P_0$ state obtained above $\omega_1^{(e)}/2\pi = 0.73$ MHz and $\omega_2^{(e)}/2\pi = 1.12$ MHz deviate from the values of $\omega_1^{(e)}/2\pi = 1.51$ MHz and $\omega_2^{(e)}/2\pi = 1.27$ MHz which we had estimated previously using $P_e = 0.42$ MHz and $\eta_e = 0.78$.[11] This estimate was based on an extrapolation of data obtained by Lee et al.[26] in their nuclear quadrupole resonance (NQR) experiments on La in LaF$_3$ above 88 °K, taking into account the known ratio of the nuclear quadrupole moments of Pr and La. Our result indicates that the crystal field at the La site has been distorted appreciably by the oversized Pr^{3+} ion. It should be remarked, however, that it is not quite clear how to extrapolate the electric quadrupole resonance (EQR) data between 88 and 3 °K, without some improvement in the theory of Lee et al.[26] describing the temperature dependence of the interaction parameters. Our inference based on our

present work that the largest component ($\hat{z}$) of the field-gradient tensor lies perpendicular to $\hat{C}_2$ is, however, consistent with the analysis of Andersson *et al.*[27] Our present work provides information only for the relative orientation of the principal axes; their absolute direction with respect to the crystal $\hat{c}$ axis can best be determined by studying photon-echo-modulation in an external field.

The $^3P_0$ excited-state splittings of 0.73 and 1.12 MHz which we now report are very close to the values of 0.75 and 1.13 MHz which we have recently reported.[12] The slightly changed values are the result of increased accuracy and resolution due to improvement in apparatus and experimental technique. Very recently Morsink and Wiersma[13] have reported echo-modulation experiments for the $^3H_4$-$^3P_0$ transition and they have inferred a excited-state Hamiltonian with $P_e = 0.096$ MHz and $\eta_e \approx 3$. This Hamiltonian leads to excited-state splittings of 0.77 and 0.38 MHz which differ considerably from ours. We note, however, that their echo-modulation data show considerably less detail than either our data or a calculation

based on the Hamiltonian that they, or we, propose.

In conclusion, we have shown that the technique of photon echoes is capable of high spectral resolution in investigating the hyperfine structure of the optically excited states of ions in solids. We have also demonstrated how a Fourier analysis yields directly the nuclear-level splittings and their associated linewidths in the terminal levels of the echo transition. In addition, because of the fact that photon echoes are produced by atoms in a linear superposition of the ground and excited states, we have been able to determine the relative orientation of the principal axes of the interaction Hamiltonians for the $^3H_4$ and $^3P_0$ states in $LaF_3:Pr^{3+}$.

ACKNOWLEDGMENT

---

[1]W. M. Yen, W. C. Scott, and A. L. Schawlow, Phys. Rev. A **136**, 271 (1964).

[2]Von M. Mansmann, Z. Anorg. Allg. Chem. **331**, 98 (1964).

[3]A. Zalkin, D. H. Templeton, and T. E. Hopkins, Inorg. Chem. **5**, 1466 (1966).

[4]N. Takeuchi and A. Szabo, Phys. Lett. A **50**, 316 (1974).

[5]N. A. Kurnit, I. D. Abella, and S. R. Hartmann, Phys. Rev. Lett. **13**, 567 (1964).

[6]N. Takeuchi, J. Luminesc. **12/13**, 743 (1976).

[7]Y. C. Chen and S. R. Hartmann, Phys. Lett. A **58**, 201 (1976).

[8]S. Kern and P. M. Raccah, J. Phys. Chem. Solids **26**, 1625 (1965).

[9]L. E. Erickson, Opt. Commun. **21**, 147 (1977).

[10]L. E. Erickson, Phys. Rev. B **16**, 4731 (1977).

[11]Y. C. Chen, K. Chiang, and S. R. Hartmann, Opt. Commun. **26**, 269 (1978).

[12]Y. C. Chen, K. Chiang, and S. R. Hartmann, Opt. Commun. **29**, 181 (1979).

[13]J. B. W. Morsink and D. A. Wiersma, Chem. Phys. Lett. **65**, 109 (1979).

[14]R. G. DeVoe, A. Szabo, S. C. Rand, and R. G. Brewer, Phys. Rev. Lett. **42**, 1560 (1979).

[15]R. M. Shelby, C. S. Yannoni, and R. M. Macfarlane, Phys. Rev. Lett. **41**, 1739 (1978).

[16]A. Yamagishi and A. Szabo, Opt. Lett. **2**, 160 (1978).

[17]A. Flusberg, T. Mossberg, and S. R. Hartmann, Opt. Commun. **24**, 207 (1978).

[18]S. Meth and S. R. Hartmann, Opt. Commun. **24**, 100 (1978).

[19]P. F. Liao, P. Hu, R. Leigh, and S. R. Hartmann, Phys. Lett. A **41**, 285 (1972).

[20]M. Littman and H. Metcalf, Appl. Opt. **17**, 2224 (1978).

[21]D. Grischkowsky and S. R. Hartmann, Phys. Rev. B **2**, 60 (1970).

[22]W. B. Mins, Phys. Rev. B **3**, 2840 (1971).

[23]L. O. Lambert, Phys. Rev. B **7**, 1834 (1973).

[24]B. Bleaney, Physica (Utrecht) **69**, 317 (1973); J. Appl. Phys. **34**, 1024 (1963).

[25]F. L. Aukhadeev and I. S. Konov, Sov. Phys. Solid State **15**, 1929 (1974).

[26]K. Lee, A. Sher, L. O. Andersson, and W. G. Proctor, Phys. Rev. **150**, 168 (1967).

[27]L. O. Andersson and W. G. Proctor, Z. Krist. **127**, 366 (1968).